

Supporting Information

Towards Lysozyme Nanotubes and 3D Hybrids Self-Assembly

Cecile Lara, Stephan Handschin, and Raffaele Mezzenga

Table of Contents:

I. Cryo-SEM nanotubes and helical ribbons images	2
II. AFM nanotubes and helical ribbons height images	4
III. FTIR deconvolution curves.....	6
IV. AFM height and amplitude images of nanotubes coated with gold nanoparticles	7
V. AFM height images of gold platelets synthesized in nanotubes and ribbons solution	7
VI. Materials and methods	8
VII. Diameter calculation.....	8

I. Cryo-SEM nanotubes and helical ribbons images

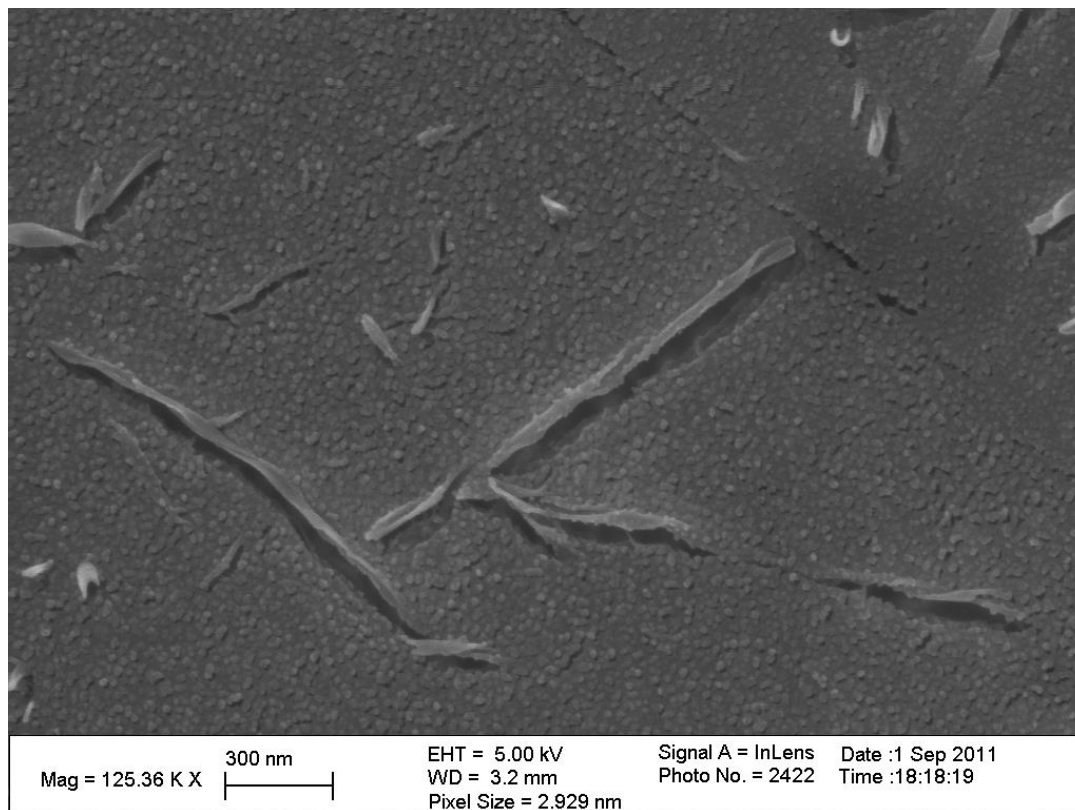


Figure S1. Cryo-SEM image of HEWL nanotubes and helical ribbons. The scale bar represents 300 nm.

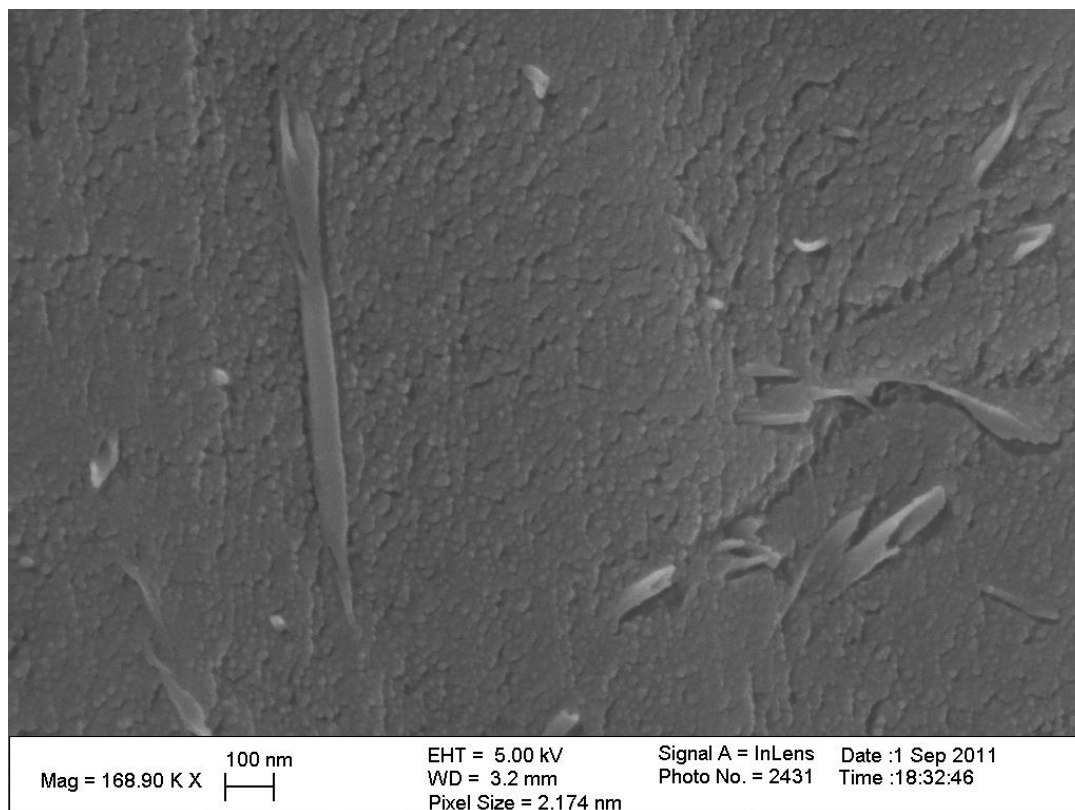


Figure S2. Cryo-SEM image of HEWL nanotubes and helical ribbons. The scale bar represents 100 nm.

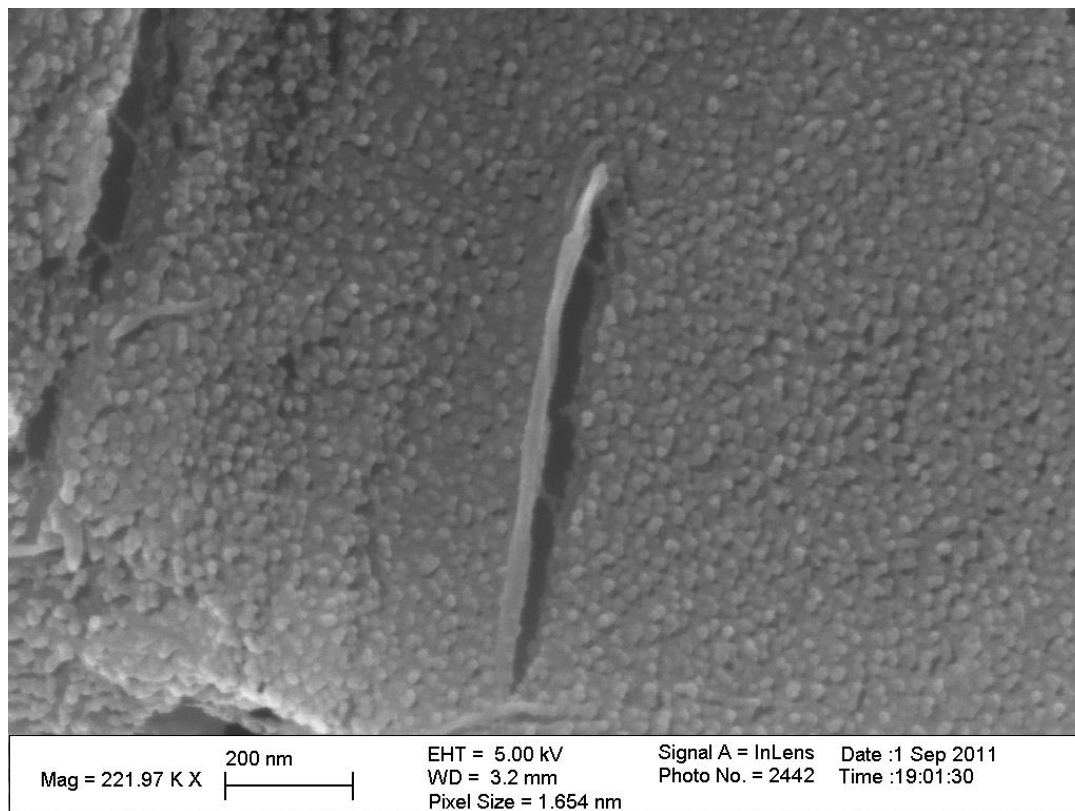


Figure S3. Cryo-SEM image of HEWL nanotube. The scale bar represents 200 nm.

II. AFM nanotubes and helical ribbons height images

The closed nanotubes are found among unclosed helical ribbons. Some already-formed nanotubes also show some breaking upon deposition on mica and drying before imaging.

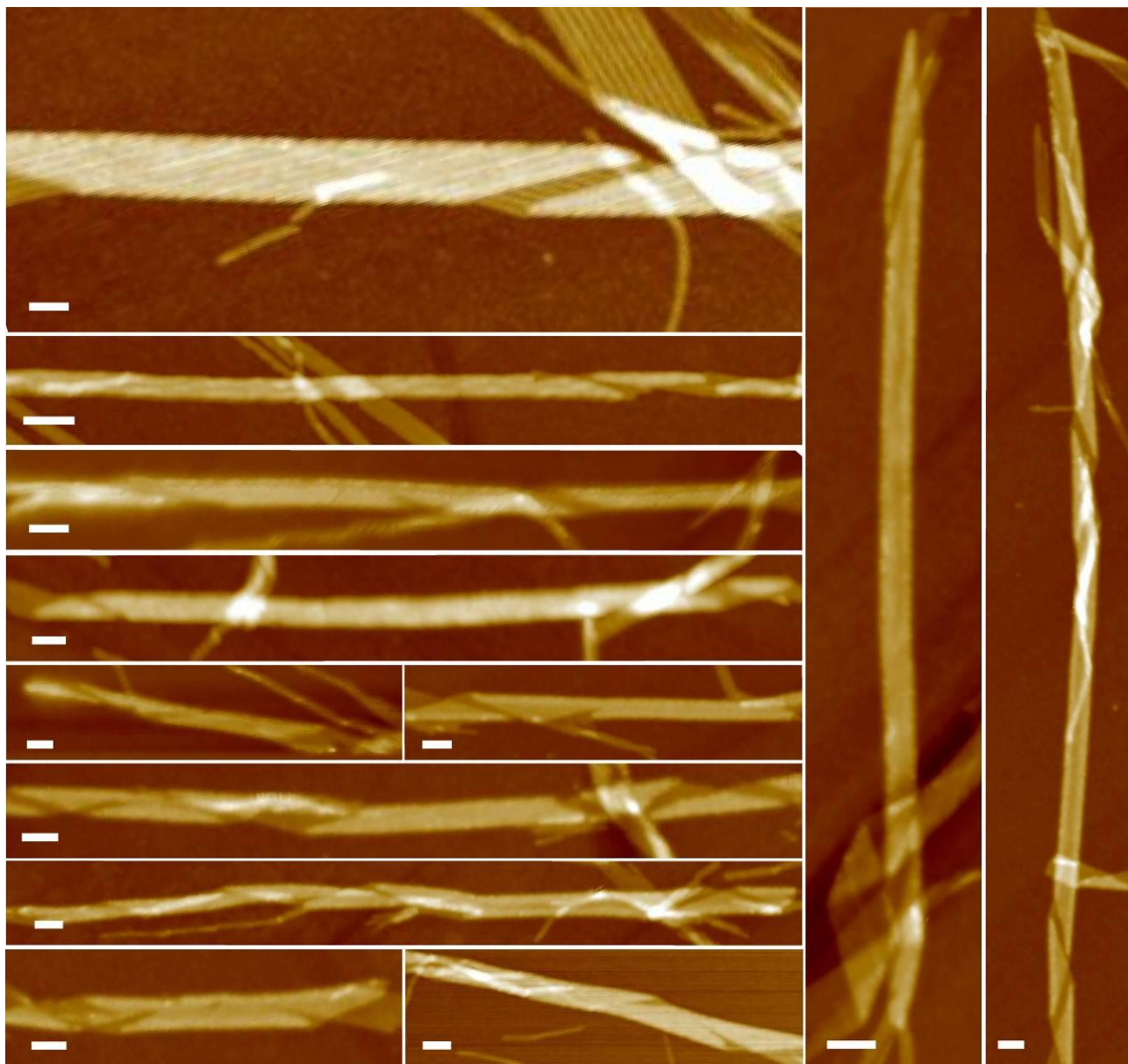


Figure S4. AFM height dry state images of HEWL nanotubes deposited on mica. The scale bars represent 100 nm. The height scales are 30 nm.

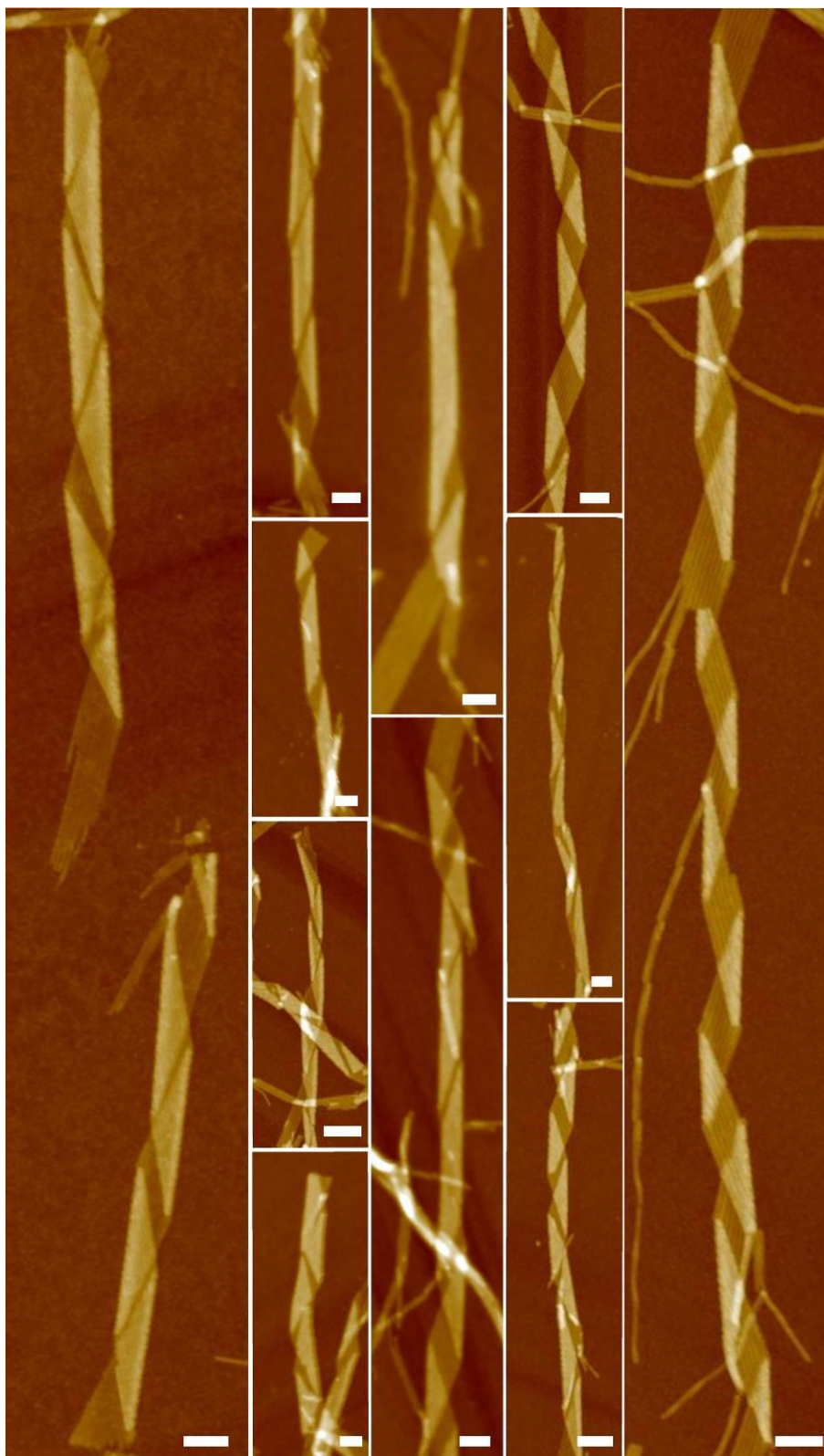


Figure S5. AFM height dry state images of HEWL nanotubes (broken when deposited and dried) and helical ribbons deposited on mica. The scale bars represent 100 nm. The height scales are 30 nm.

III. FTIR deconvolution curves

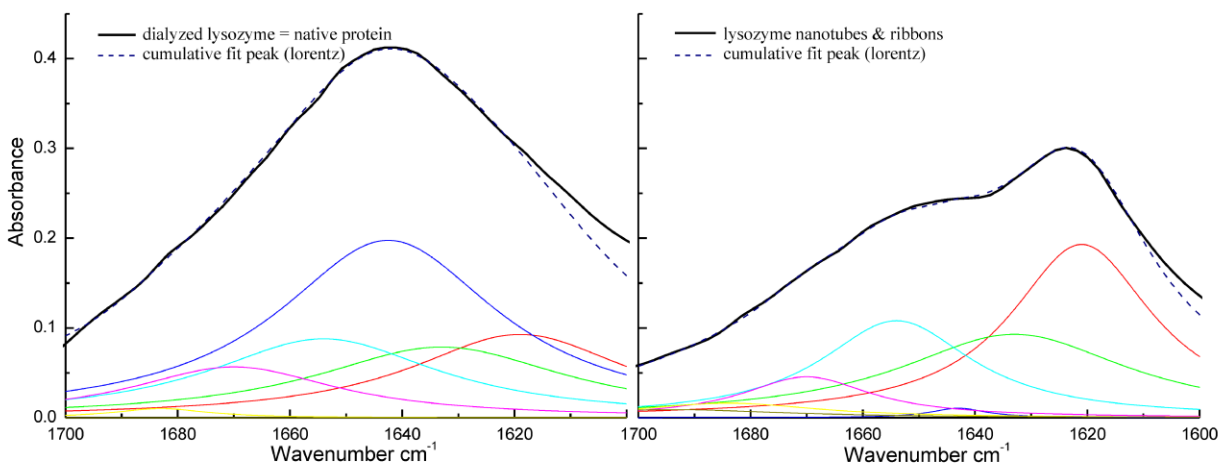


Figure S6. FTIR absorbance spectra of the native protein (left) and the amyloid-like nanotubes and helical ribbons mixture (right) in the amide I wavenumber range.

	Nanotubes + Helical ribbons		Native HEWL		Nanotubes + Helical ribbons		Native HEWL
Peak 1 <i>Cross-β</i>	xc	1621	1619	Peak 5 <i>β-turn</i>	xc	1670	1670
	w	31	48		w	28	45
	A	9.4	7		A	2	4
Peak 2 <i>β-sheet</i>	xc	1633	1633	Peak 6 <i>Anti-parallel</i>	xc	1684	1683
	w	50	55		w	39.1	20
	A	7.3	6.8		A	1	0.3
Peak 3 <i>Random coil</i>	xc	1643	1643	Peak 7 <i>β-turn</i>	xc	1694	1694
	w	12	48		w	50	10
	A	0.2	14.9		A	0.7	0
Peak 4 <i>α-helix</i>	xc	1654	1654	Fitting equation: $y = (2A/\pi) * (w / (4(x-xc)^2 + w^2))$			
	w	33	50				
	A	5.6	6.9				

Table S11. Deconvolution peaks maxima (xc) and their corresponding width (w) and area (A) when fitted with a “Lorenz” distribution and the corresponding secondary structure attribution.

IV. AFM height and amplitude images of nanotubes coated with gold nanoparticles

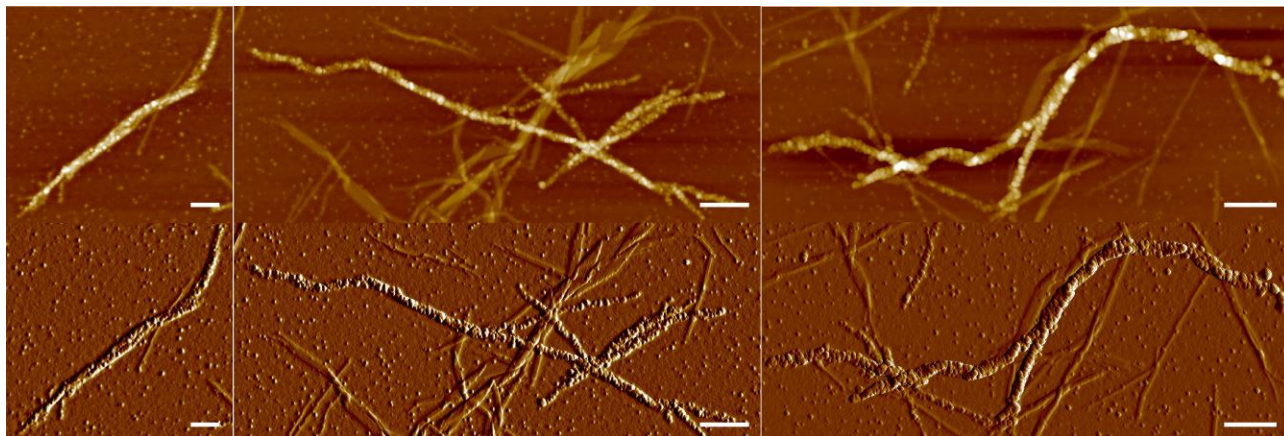


Figure S7. AFM height images (top line) and amplitude images (down line) of HEWL fibrillar assemblies covered with gold nanoparticles after addition of gold salt and reducing agent in the fibrils solution. The scale bars represent 200 nm. The height scales are from left to right 40 nm, 60 nm and 80 nm respectively.

V. AFM height images of gold platelets synthesized in nanotubes and ribbons solution

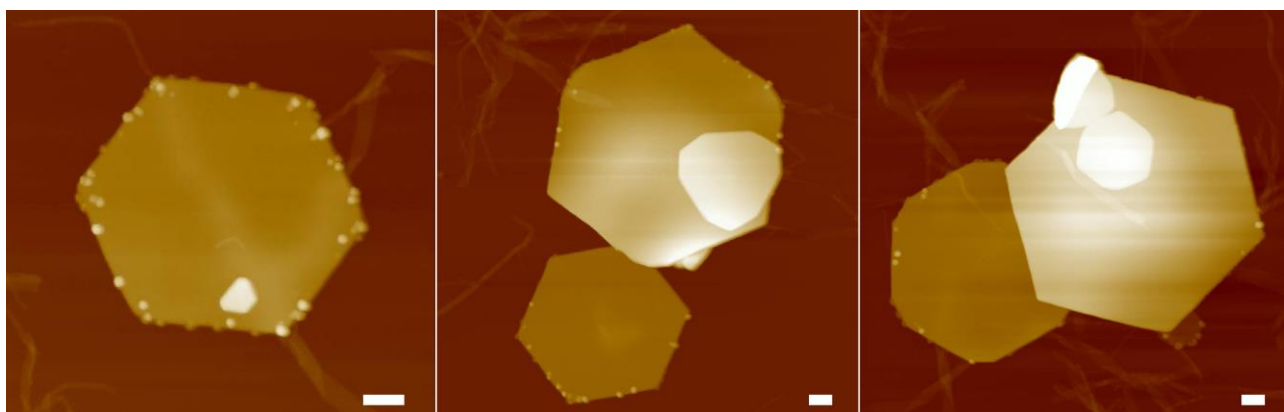


Figure S8. AFM height images of HEWL nanotubes and helical ribbons inducing the formation of gold micro crystals. The scale bars represent 200 nm. The height scales are from left to right 150 nm, 250 nm and 250 nm respectively.

The fibrillar aggregates, containing cysteine residues that are more reactive than in the native folded protein conformation, can act as a reducing agent of the gold salt and as capping agent. A nucleation and growth process, templated by the gel-like fibrillar network, is thought to occur in a similar way than reported for the BSA protein denatured by heat treatmentⁱ and has been already reported in beta-lactoglobulin amyloid fibrils in our earlier work.ⁱⁱ

VI. Materials and methods

The HEWL helical ribbons were formed as previously reported.ⁱⁱⁱ Closure into nanotubes is observed after two weeks of storage of the 2 wt% solution at 4°C.

The Atomic Force Microscopy (AFM) images were collected using a Nanoscope VIII Multimode Scanning Force Microscope (Bruker) operated in tapping mode in air and flattened using the Nanoscope 8.10 software. Wide Angle X-ray Scattering (WAXS) experiments were performed on a Micro Max-002+ microfocussed beam with a sealed tube Cu K α ($\lambda = 1.542 \text{ \AA}$) source, collimated by three pinhole collimators (0.4, 0.3, and 0.8 mm), the applied voltage and filament current being 45 kV and 0.88 mA, respectively. The data were collected with the help of a Fuji Film BAS-MS 2025 imaging plate system: 15.2 \times 15.2 cm, 50 μm resolution.

The Circular Dichroism (CD) and Fourier Transform Infra-Red (FTIR) measurements were run on a Jasco J-815 spectrometer and a Varian 640 FTIR Spectrometer respectively, following the same procedure described in our previous work.^{iv}

For cryo-SEM experiments, a few μL of the sample were sandwiched between two flat 6 mm aluminium specimen carriers with 100 μm cavity and immediately high-pressure frozen (HPM 100; Bal-Tec/ Leica). The two carriers were then mounted under liquid nitrogen on the specimen holder (VCT 100 cryopreparation box, BAF 060 freeze-fracturing device Bal-Tec). The fractured surfaces were etched at -95°C for 5 min in vacuum ($\sim 10^{-7}$ mbar) and then coated with 4 nm tungsten by electron beam evaporation. The samples were transferred on the cryostage in the SEM (Leo Gemini 1530; Zeiss, Oberkochen, Germany). Samples were imaged at -120 °C at an acceleration voltage of 2 kV using the in-lens secondary electron detector.

VII. Diameter calculation

Considering a totally flattened nanotube (bilayer), the width measured by AFM, $w=95 \text{ nm}$, represents half of the external circumference.

One can thus write: $2w = 2\pi r$

which gives $d = 2r = 60.5 \text{ nm}$ external diameter (approximated to 60 nm in the manuscript).

ⁱ M.S. Bakshi, H. Kaur, P. Khullar, T.S. Banipal, G. Kaur and N. Singh, *J. Phy. Chem. B*, 2011, **115**, 2982-2992.

ⁱⁱ S. Bolisetty, J.J. Valooran, J. Adamcik, S. Handschin, F. Gramm and R. Mezzenga, *J. Colloid Interf. Sci.*, 2011, **361**, 90-96.

ⁱⁱⁱ C. Lara, J. Adamcik, S. Jordens and R. Mezzenga, *Biomacromolecules*, 2011, **12**, 1868-1875.

^{iv} C. Lara, S. Gourdin-Bertin, J. Adamcik, S. Bolisetty and R. Mezzenga, *Biomacromolecules*, 2012, **13**, 4213-4221.